A Comparison of Coreflood and Digital Rocks Methods to Study the Remobilisation of Residual Gas Through Depressurisation

Chris Jones[1,*], *Vahid* Azari[1], *David* Rodrigues[1], *Pavel* Gramin[1], *Glen* Gettemy[1], *Yang* Ning[1], *Nazim* Abdullayev[1], *Araz* Khalafli[1] and *Denis* Klemin[2]

[1] BP, Sunbury on Thames, UK.
[2] SLB, Houston, Tx, USA.

Abstract. A series of coreflood experiments were conducted as part of a broader study of the remobilisation of trapped gas. A well drilled beneath the producing zones logged hydrocarbon gas saturations of up to 50% in sandstones of comparable rock quality to the overlying zones. A subsequent well test found that only the brine phase flowed, suggesting that the hydrocarbon gas is in an immobile, residual state. To assess the feasibility of producing gas from this residual zone, a Digital Rocks (DR) study was devised to replicate the complex reservoir behaviour and evaluate the mechanisms that occur as brine is produced under pressure depletion until the immobile gas phase starts to flow. DR was chosen to study this process because the pore pressure in the exploration well was ~20,000 psi, higher than the maximum operating pressure of the coreflood equipment available. To test the validity of the DR model, a series of corefloods was performed at reduced pressure using model fluids. One coreflood was designed to mimic the reservoir mechanisms as closely as possible, while a second was modified to allow a robust comparison with the DR simulations. The DR model was validated by successfully replicating the laboratory tests so that it could be used to predict gas remobilisation at full reservoir conditions using hydrocarbon gas.

1 Introduction

In 2023, an exploration well was drilled by BP to target deep untested resources with the aim of exploring potential resources in a previous unpenetrated part of the field. An extensive data acquisition programme was run, including Logging While Drilling (LWD), formation pressure and wireline fluid sampling. The planned sidewall core (SWC) programme could not be completed because the liner needed to be set to isolate the open hole due to wellbore instability.

The well penetrated wet sands with hydrocarbon saturations of up to 50%. The hydrocarbons were interpreted to be a discontinuous, immobile gas phase trapped by a mobile water phase. This interpretation was supported by fluid samples taken on wireline, where only brine was found to flow. The trapped gas is believed to have been formed due to a seal leak.

A study was undertaken to determine whether the residual gas could be remobilised efficiently by depressurisation, to inform field development decisions.

Due to the lack of SWC from the potential reservoir sections in question, core was used from one of the producing sandstone reservoirs above the target. Because pore size and pore connectivity have a significant effect on trapped gas saturation, great care was taken to select representative core which closely matched the petrophysical properties seen from LWD data [1]. The selection criteria included log porosity and permeability, mineralogy, cementation and core heterogeneity.

Due to the high reservoir pore pressure (~20,000 psi) and temperature (~100 ºC) a three-phase approach was adopted:

1) Laboratory coreflood experiments were conducted using analogous reservoir rock at 60 °C and 4,000 psi, as the actual reservoir pressure exceeded laboratory equipment limitations.

2) Digital Rocks (DR) pore-scale simulations were first validated by replicating the coreflood results using model fluids and reduced conditions, then repeated to model hydrocarbon gas behaviour at true reservoir conditions.

3) Reservoir-scale material balance tank modelling was used to forecast field performance during gradual water production and pressure drawdown.

The critical gas saturation (S_{gt}), the saturation where trapped gas is remobilised and flows, has been shown to be higher than the maximum trapped gas saturation (S_{gr}) achievable by an imbibition waterflood [2]. Moghadasi et al. [3,4] demonstrated the counter intuitive result that mobilised gas relative permeability is reduced as gas saturation increases during depressurisation.

* Corresponding author: christopher.jones2@uk.bp.com

A previous laboratory study conducted using conventional, centimeter scale coreplugs, with similar initial trapped gas saturations to those observed in this study, found that S_{gt} was 3% higher than the initial S_{gr} [5]. The same paper reported that after depressurisation from 1,700 psi to 500 psi, 70 % of the initial trapped gas had been produced.

2 Coreflood Materials & Methods

2.1 Fluid and Core Preparations

The reservoir pore pressure in the logged intervals was ~20,000 psi and ~100 °C and the gas in place is believed to be predominantly methane. The pore pressure in the DR simulations was reduced by 10,000 psi, a greater drop than would realistically be conducted in the field, therefore covering any foreseeable development. The ratio of methane density from the start to the end of the 10,000 psi depressurisation was 1.335 and for viscosity ratio was 1.532.

The corefloods in this study used nitrogen gas in-place of hydrocarbons, as the coreflood rig available was unable to use flammable gasses. The constant temperature used and the pore depressurisation range was chosen so the density ratio over the depressurisation range exceeded that of the DR simulations with methane gas, as shown below in **Table 1**. It was not possible to match the reservoir viscosity ratio with available fluids.

Table 1 : Density and viscosity ratios of nitrogen used in core floods at 60 °C

Pore Pressure (Psi)	Density (g/cc)	Viscosity (cP)
4,000	0.246	0.026
2,300	0.153	0.023
Ratio (4,000 : 2,300)	1.611	1.151

The brine used was a simplification of the reservoir fluid, with the addition of 50 g/l of NaI to replace NaCl at the equivalent molar concentration. This was done to increase the x-ray attenuation contrast between brine and gas phases. The iodide doped brine had a TDS of 61,000. The viscosity and density of the brine during the depressurisation corefloods at 60 °C is shown below in **Table 2**.

Table 2 : Viscosity and density of doped brine fluid

Pressure (psi)	Viscosity (cP)	Density (g/cc)
4000	0.535	1.036
2300	0.531	1.031

Twenty core plugs were cut from whole core pieces from a cored interval of an offset well. CT images, porosity, and permeability measurements were used to select three well matched plugs used to form a composite core. A composite was used to increase the initial trapped gas volume, thereby increasing potential production volume. The harmonic mean of the three individual core plug permeabilities was 51.1 mD, the sum of the three pore volumes (PV) was 26.0 ml and the average porosity was 11.9 %. The composite was 19.1 cm long and had a cross-sectional area of 11.25 cm^2. The composite core was wrapped in PTFE tape and heat shrink material to protect it from grain loss.

2.2 Coreflood Design

Consider a sandstone reservoir containing a trapped gas phase being depressurised by producing brine. The overburden pressure acting on the reservoir is constant, and so during pore pressure reduction, the Net Confining Stress (NCS) increases. Increasing NCS during depressurisation squeezes pores and pore throats, changing their shape and size, which may have a significant effect on the reconnection and flow behaviour of a residual gas phase.

The microplugs imaged for the DR study were in an unstressed state and so the reconstructed 3D model of the pore space used in subsequent simulations was of fixed geometry throughout. The purpose of the corefloods was to validate the DR simulation models and to provide a physical test of whether the DR simulation process accurately captured the physics of gas remobilisation during depressurisation. Three corefloods were designed to address these needs.

Coreflood 1: A close analogue to the DR model, where NCS remained constant during pore depressurisation.

Coreflood 2: Identical to Coreflood 1, but no coreplug was loaded. The objective was to understand the contribution of gas exsolution from brine in the rig pipework to the measured gas production.

Coreflood 3: Identical to Coreflood 1 but a closer analogue to the reservoir, where NCS increased during pore depressurisation.

All floods were conducted at 60 °C using identically prepared live brine and humid nitrogen. All started at 4,000 psi pore pressure with the nitrogen and brine phases at equilibrium, ensuring that there was no mass transfer between the gas and liquid phases at the start of the floods. The pore pressure was reduced at a constant rate of 174 psi per day in each flood. Overburden pressure started at 4,500 psi in all cases, and for Coreflood 3 this was also reduced at 174 psi per day.

If a well penetrating a residual gas zone were drawn down, brine would be expected to flow before trapped gas is remobilised and produced. This behaviour was replicated in the corefloods by continual recirculation of equilibrium brine upwards through the core at 2 ml/hr during depressurisation. The capillary number (N_c) associated with this flow rate was calculated to be 4.4x10^{-7} at the start of the depressurisation, when gas was immobile, and the interfacial tension between the brine and nitrogen was 0.05 N/m.

The corefloods were conducted on a steady state coreflood rig with an x-ray in-situ saturation monitoring (ISSM) system. Fluids were recirculated using twin syringe pumps to the core, then through an Anton Paar DMA HPM density meter, then back into a two-phase acoustic separator.

2.2.1 Coreflood 1: close analogue to DR simulations, constant NCS

The first coreflood experiment was designed to validate the DR models. This meant that NCS was held at a constant, low value throughout. To achieve this, piston vessels containing nitrogen gas on the process side and water on the driven side were connected to both the core confining pressure system and the pore pressure system. Water was withdrawn from the driven sides of both piston vessels using dedicated Quizix syringe pumps. The pump software maintained a depressurisation rate of 174 psi per day for both pore and confining circuits. The setup is shown below, in Fig. 1.

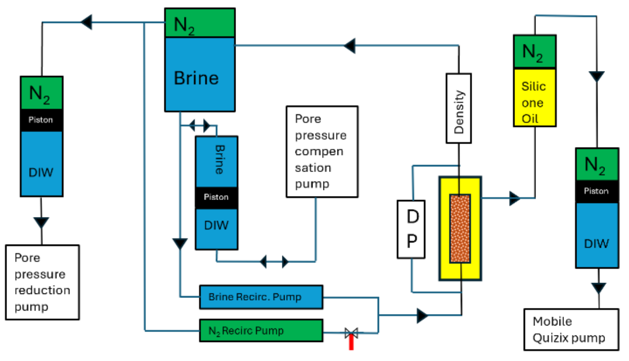

Fig. 1: Coreflood 1 equipment schematic

The composite core was inserted into a viton rubber sleeve then mounted in an x-ray transparent carbon fibre core holder. The composite core was degassed with dead brine then brought to the coreflood pressure and temperature before flushing with 100% live brine. ISSM calibration data were recorded. The composite was then cleaned to 100% nitrogen by flowing 10 PVs each of isopropanol, toluene, pentane, and dry nitrogen in sequence. Dry nitrogen was displaced with humid nitrogen, and the second 100% phase ISSM calibration recorded.

To set up the trapped gas saturation a low-rate brine imbibition flood was conducted upwards at 2 ml/hr until ISSM saturation data indicated no further saturation change, differential pressure (DP) across the core had plateaued and inline density measurement was stable. Immediately after the stable trapped gas saturation (S_{gr}) was achieved, the depressurisation test was started. Pore and overburden pressures were simultaneously reduced at a constant rate of 174psi per day for 10 days. During the depressurisation, brine continued to be recirculated at 2 ml/hr. The capillary number, the ratio of viscous to capillary forces in the fluid system is calculated by:

$$N_c = \frac{u_w . \mu_w}{\Phi . \sigma}$$

u_w= velocity of the brine front flowing through the rock (m/s)
μ_w= viscosity of the live brine (Poise)
Φ = porosity (unitless)
σ = interfacial tension between brine and nitrogen (N/m)

The fluid velocity u_w is calculated by:

$$u_w = \frac{Q}{A}$$

Where:
Q=volumetric flow rate of brine through the rock (m^3/s)
A=the cross-sectional area of the core plug in m^2

The composite core had an average cross-sectional area of 11.25 cm^2, and porosity of 0.12. An accepted industry-standard value for the interfacial tension between nitrogen and brine is 0.05 N/m, and the viscosity of the brine at 60°C and 4,000 psi is 0.00535 Poise. This meant that at the initial flowing conditions, Coreflood 1 had a capillary number of 4.4×10^{-7}. The viscosity change of the brine by the end of the depressurisation was very small (0.00535 down to 0.00531 Poise), so the capillary number change throughout was negligible.

Coreflood 1 had a constant NCS throughout the depressurization. However, a positive NCS is required throughout the test to ensure the rubber sleeve surrounding the core sample forms a seal between the fluids inside the pore space and the confining fluid surrounding it. From BP experience, a minimum NCS of 500psi is required to maintain reliable separation between pore and confining fluids.

2.2.2 Coreflood 2: no core plug

The purpose of this test was to understand the contribution to total produced gas from nitrogen exsolved from the live brine in the pipework of the rig, as opposed to nitrogen originating in the core plug. The core holder end pieces were placed together and fitted with a rubber sleeve to keep them separated from the overburden fluid. All rig pipework was filled with live brine fluid at 60 °C at 4,000 psi, and a confining pressure of 4,500 psi was applied. The core holder was opened to the density meter, separator and recirculation pump circuit, and live brine recirculation started at 2 ml/hr (i.e., the same flow path as Coreflood 1). The pore pressure was reduced at a rate of 174 psi per day, for a total of 10 days.

2.2.3 Coreflood 3: replicate reservoir processes: increasing NCS

This coreflood was identical to Coreflood 1, except that the overburden pressure remained constant at 4,500 psi throughout. The external piston vessel and withdrawal pump were removed from the confining system, otherwise the coreflood rig setup was the same. Coreflood 3 was run at identical conditions and rates to Coreflood 1. This setup is illustrated below in Fig. 2:

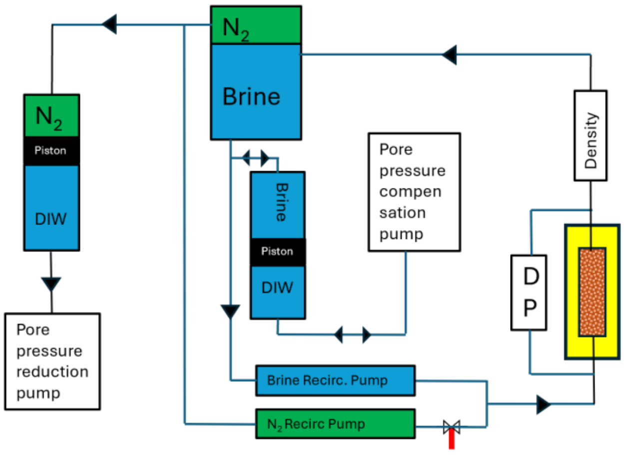

Fig. 2: Coreflood 3 equipment schematic

2.3 Density analysis

An Anton Paar DMA HPM densitometer was installed in line between the core outlet and the final separator, which was housed in the coreflood rig oven in temperature equilibrium with all other components, enabling continuous, real-time monitoring of fluid density during floods. The instrument is built around a high-precision U-tube oscillation cell, which resonates at a frequency dependent on the density of the fluid passing through it, hence the densitometer captures the immediate density response of the effluent stream from the core.

During depressurisation tests, the densitometer captured the signature density “kicks” that correspond to produced gas slugs from the two-phase stream. These readings formed the basis for converting density-time profiles into quantitative gas production, using the density of pure phases:

$$\rho_{\text{mix}} = \phi_g \rho_g(P,T) + (1 - \phi_g)\rho_w(P,T)$$

where ρ_{mix} is the measured outlet density and ϕ_g is the gas volume fraction. Pure densities ρ_g and ρ_w were measured at 2000, 3000 and 4000 psi and interpolated for test pressures in between. Given the exact injection rate, the gas volume at each increment was calculated using gas fraction values and these volumes were converted to cumulative gas production by taking an integral over the entire depressurisation. This technique was adapted from that described in [6] and can be described mathematically as:

$$G_{\text{cum}}(P) = \int V_g(P)\, dP$$

where

$$V_g = \phi_g \times V_t$$

and

$$V_t = Pump\ Injection\ Rate \times dt$$

2.4 ISSM saturations during depressurisation

X-ray radiation from the source in the ISSM system is attenuated by all materials between it and the detector panel. The degree of attenuation is related to the density and thickness of the material and the atomic mass of the atoms of which it is made. All these factors control the total cross-sectional-area of atomic nuclei which fall in the path of the x-rays.

A cross section through the x-ray beam path during the corefloods is shown below in Fig. 3. The materials in the path are the carbon fibre barrel of the core holder (black in the illustration), the silicone oil confining fluid (yellow), the rubber sleeve surrounding the core (blue) and the core plug itself (orange). Not shown in the picture are the fluids contained within the pore space of the rock. The difference in attenuation through the varying fluids within the pore space are the only variables in corefloods conducted at constant temperature and pressure using two immiscible fluids. Fluid saturations during flooding are calculated by comparing the x-ray attenuation at any given saturation with the attenuation measured with the pore spaced entirely filled with each of the two phases. In a brine/nitrogen system, the average brine saturation, Sw, in the volume of interest is calculated by:

$$S_w\,(x) = \frac{(\mu_{Nitrogen} - \mu_{mix})}{(\mu_{Nitrogen} - \mu_{Brine}\,)}$$

where μ denotes the attenuation of x-rays measured with either pure nitrogen, brine, or mixture of both in any proportion at the point of interest during the coreflood.

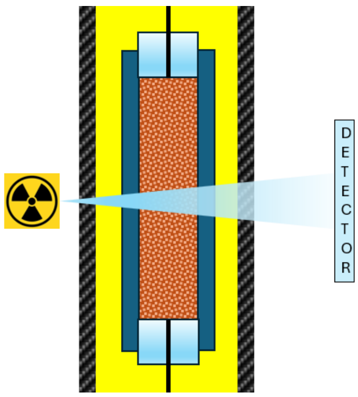

Fig. 3: Cross section of core holder showing x-ray beam path

During ISSM calibrations, x-ray attenuation was measured at varying pore pressure with a constant net overburden of 500 psi, for both brine and nitrogen fluids. X-ray attenuation for 100% brine saturation at varying pore pressure and constant net overburden are shown in Fig. 4. The attenuation measured at five pressures, covering the range of the corefloods, did not vary significantly, with the five curves overlying one another. The sixth (green) dataset shows the x-ray attenuation at 100% nitrogen saturation at the highest pore and overburden pressures used in the corefloods, which is clearly lower than the brine attenuations. During the constant net overburden depressurisations, both the fluid in the pore space and the silicone oil confining fluid reduce in density, which will reduce x-ray attenuation. However, as these results demonstrate, this change is unmeasurable compared to the difference in attenuation between brine and nitrogen phases at any pressure within the range of the corefloods detailed in this report.

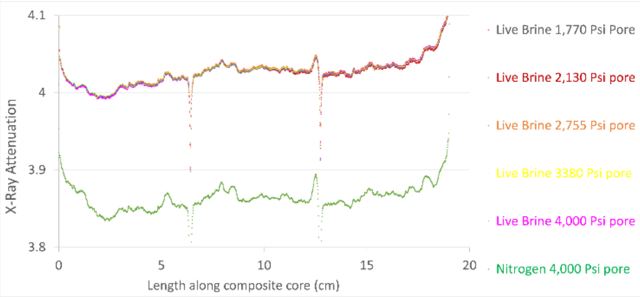

Fig. 4: X-ray attenuation at 100% nitrogen and 100% brine saturation at varying pore and overburden pressures, all with 500 psi NCS.

For the initial stages of each coreflood, where the pore and overburden pressures are constant and equal to those of the 100% phase calibrations, the ISSM saturations will be fully quantitative. As pressures are reduced, the findings above suggest that the calculated brine and nitrogen saturations will remain close to quantitative, although some uncertainty will remain due to the known effect of density on x-ray attenuation.

3 Discussion of Coreflood results

3.1 Coreflood 1 – constant NCS

The composite coreplug was initially 100% saturated with gas, and then brine was injected until the ISSM saturation profile was stable, as shown below in Fig 5. The different datasets show the brine flood front progressing upwards through the composite core (right to left on the chart) as brine is injected. As the front progressed upwards through the core, near constant water saturation was left behind as a localised trapped gas saturation was reached. The average S_{gr} across the composite was 0.53 PV.

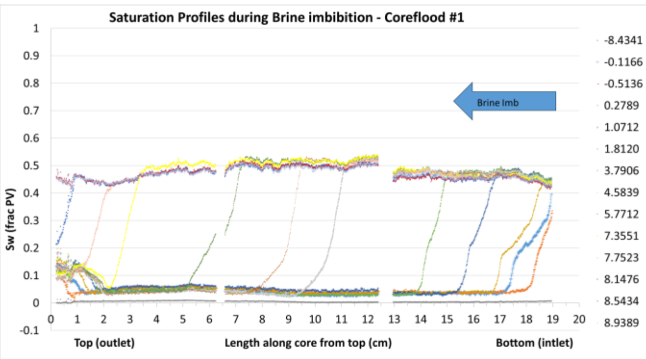

Fig 5*:* Initial in-situ water saturation before depressurisation

Once the stable S_{gr} of 0.53 PV was reached, the depressurisation began. The pore and overburden pressures throughout the coreflood, showing a stable NCS of 500 psi, are shown below in Fig 6 (orange and grey lines). The brine relative permeability to brine is shown as blue and represents the brine permeability compared to the absolute permeability to brine.

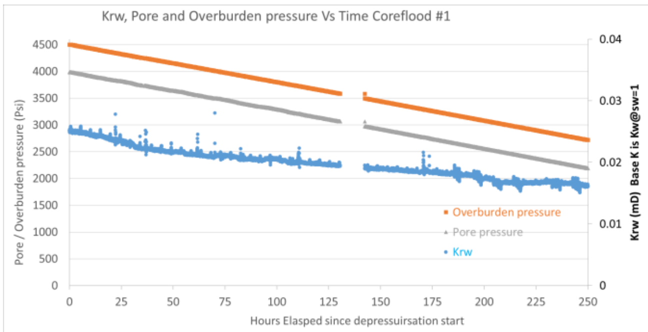

Fig 6: Pore and overburden pressure and water relative permeability (k_{rw}) during Coreflood 1

Differential pressure (dp) data across the composite was measured during the test. As water was the only continuous phase, the dp data was assigned to the water phase to calculate the relative permeability of water k_{rw}, as shown in Fig 6. From the k_{rw} curve, water mobility initially decreases rapidly but then drops at a lower rate. The reduction in k_{rw} is likely related to initial gas expansion in the system, before gas production. There is a delay between the reduction in the rate at which k_{rw} decreases (after about 40 hours) and the first gas bubble (about 75 hours; Fig. 7). It is therefore possible that some tiny bubbles of gas were produced after 40 hours but were held up in the rig pipework between the core holder and the density meter. There, they may have coalesced into a single large droplet that passed through the density meter after 70 hours. This hypothesis needs more data to verify.

The density of effluent flowing from the core (blue line) is illustrated in Fig. 7 and is compared to the single-phase baselines for 100% brine (orange) and 100% nitrogen (green) during depressurisation.

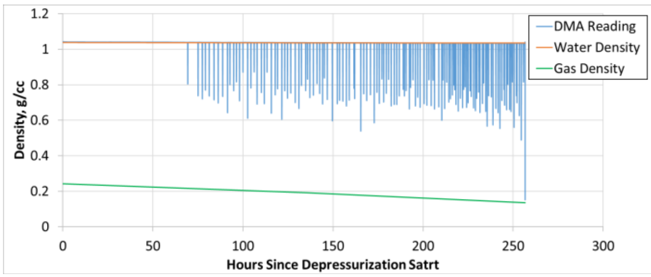

Fig. 7*:* Density readings and single-phase baselines in Coreflood 1

The chart clearly shows that 75 hours elapsed before the first nitrogen bubble reached the density meter. Correcting for the pipework volume between the outlet (top) core face and the density meter, the first nitrogen production from the core was registered at 3,501 psi pore pressure. It should be noted that gas may have mobilized inside the core at a slightly higher pressure, earlier in the depressurisation. However it was after this ~500 psi drop, from the initial pressure of 4000 psi, that free gas exited the core face. Note that the production data do not indicate continuous production of gas, instead production was via intermittent, small gas bubbles.

Using the integral approach described above in Section 2.3, the gas production volume was calculated at different stages of depressurisation. Volumes were corrected back to a constant pressure to derive the cumulative production. Using gas density data from PVT modelling, all data points were converted to an equivalent gas volume at 4,000 psi. Fig 8 shows the equivalent gas production at 4,000 psi and the cumulative production curve, which indicates an ultimate recovery factor (URF) of 33.6% of the gas initially in place (GIIP).

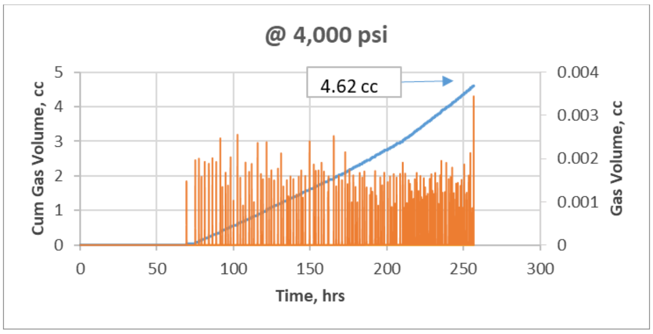

Fig 8: Gas cumulative production corrected back to 4000 psi

Water saturation (and by inference, gas saturation) is shown in Fig 9. From the initial trapped gas saturation Sgr = 0.53 PV at the starting 4,000 psi pore pressure, after 141 hours of depressurization, at 3,000 psi pore pressure, the gas saturation was 0.56 PV. At the end of the depressurization, at 2,300 psi pore pressure, the gas saturation was 0.59 PV.

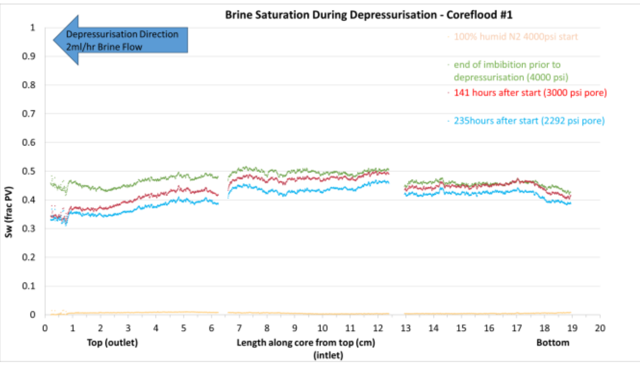

Fig 9: In-situ water saturation profile during coreflood 1

3.2 Coreflood 2 – no core plug

Coreflood 2 started with all the coreflood rig pipework filled with live, nitrogen saturated, brine. Nitrogen was present as a bulk phase only in the top of the separator. With equilibrium brine recirculating upwards through the core holder at 2ml/hr, the system was depressurised for 10 days at the same rate as the other corefloods. No nitrogen production was observed at the inline density meter. The contribution of nitrogen exsolved from the brine in the pipework of the rig to gas production measured in the other corefloods is therefore unmeasurably small, hence all gas production can be attributed to production from the core.

3.3 Coreflood 3 – increasing NCS

Coreflood 3 started with the same 2 ml/hr brine imbibition to a trapped gas saturation as Coreflood 1. The trapped gas saturation was 0.49 PV, slightly lower than the 0.53 PV in Coreflood 1. The constant overburden and reducing pore pressure during the depressurisation are shown below, in Fig. 10.

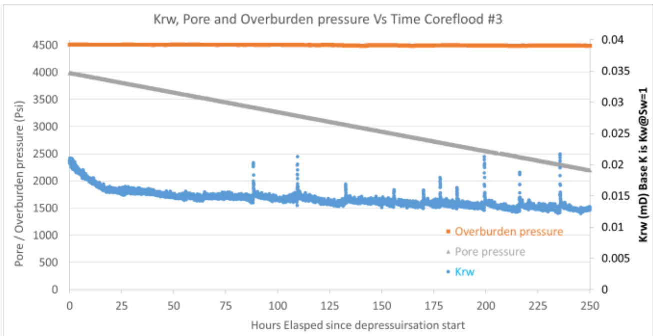

Fig. 10: Pore and overburden pressure and K_{rw} during coreflood 3

The blue line in Fig. 10 is the brine relative permeability, which showed an initial rapid decrease followed by a steadier decline. This change in rate coincided approximately with the start of gas production. Fig. 11 shows the effluent density readings throughout Coreflood 3. Compared to Coreflood 1, gas production started earlier, after only 12 hours of depressurization, when the pre pressure had dropped to just over 3,900 psi. Gas production throughout the depressurisation was higher than in Coreflood 1.

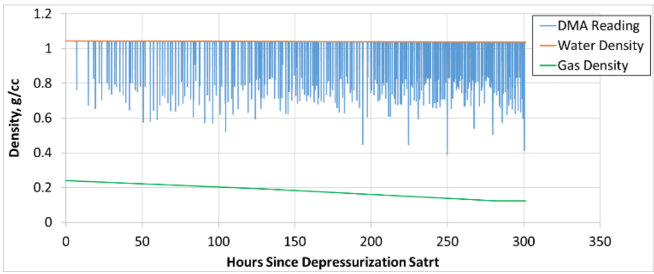

Fig. 11: Density and single-phase baselines in Coreflood 3

Coreflood 3 showed significantly higher recovery of 77.3% of GIIP, more than double that of Coreflood 1. Cumulative gas production corrected back to the initial 4,000 psi pore pressure is shown below in Fig 12.

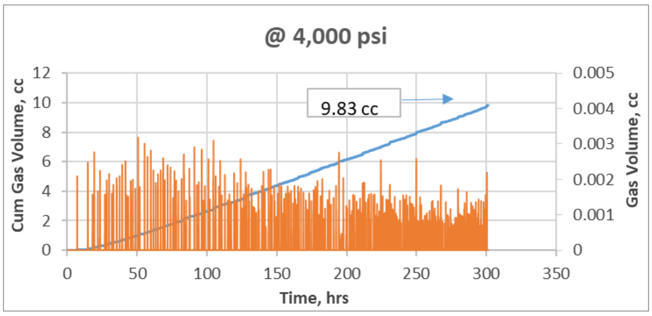

Fig 12: Gas production data at test condition (left) and equivalent cumulative production at 4,000 psi (right)

The change in gas saturation during the depressurisation is illustrated below in Fig 13. The initial Sgr at 4,000 psi pore pressure was 0.49 PV. After 141 hours of depressurisation to 3,000 psi, the gas saturation had decreased slightly to 0.48 PV. By the end of the depressurization, at a pore pressure of 2,300 psi, the gas saturation remained unchanged at 0.48 PV.

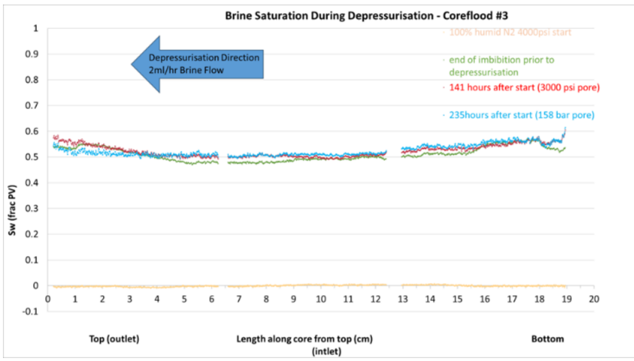

Fig 13:- In-situ water saturation profile during Coreflood 3

A possible explanation for the increased URF and only slightly reducing gas saturation in Coreflood 3, compared to the lower production and increasing gas saturation observed in Coreflood 1, relates to where within the pore space the gas and brine phases reside, and the disproportionate compaction effect of increasing net confining stress on smaller pores. A well-documented effect of increasing NCS is to compact the rock, reducing the permeability and porosity and changing the pore geometry [7]. Assuming uniform compaction, small pores are proportionally more affected by these phenomena than larger ones. As the rock in these corefloods was water wet, smaller pathways in the rock structure were predominantly filled with water. This means that compaction displaces water from small pores into larger pores, where the non-wetting gas phase predominantly resides. Hence, during compaction, the pore space becomes more favorable to holding the wetting brine phase in the increasingly small pores and throats, and less favorable to retaining non-wetting gas, which will be found in the increasingly less prevalent, larger pores.

To investigate the effect of net overburden stress on permeability, the core was fully saturated with gas and the gas permeability was measured at different levels of net overburden stress. After each 500 psi increase in NCS, the plug was left for 24 hours to settle before the permeability was measured. The readings were repeated as the NCS was reduced and were no different to the values measured as NCS increased. Fig 14 below summarises the results and shows that the permeability of the rock reduced by just over 7% over the range of NCS change during Coreflood 3. This shows that the effect of increasing NCS is significant and measurable though does not confirm the hypothesis described above is the reason for the increased recovery factor in coreflood 3 compared to coreflood 1.

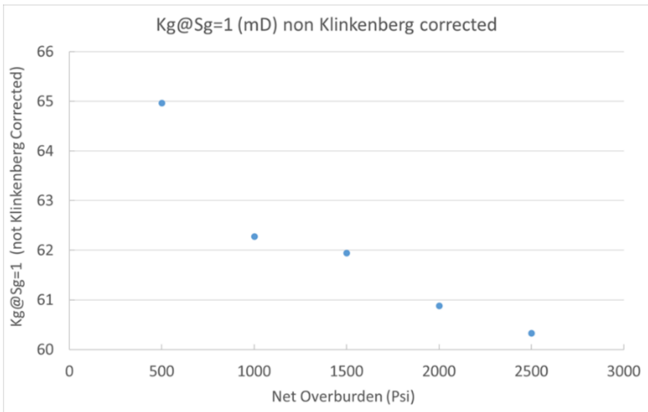

Fig 14: Permeability change of the core with increasing NCS

3.4 Numerical simulation results – Coreflood 1

Coreflood 1 was simulated using Landmark's Nexus® simulator. A 1D model was built, as shown below in Fig 15. Each of the three plugs forming the composite was represented and buffer cells were placed at either end to represent the capillary discontinuity at the inlet and outlet faces of the core.

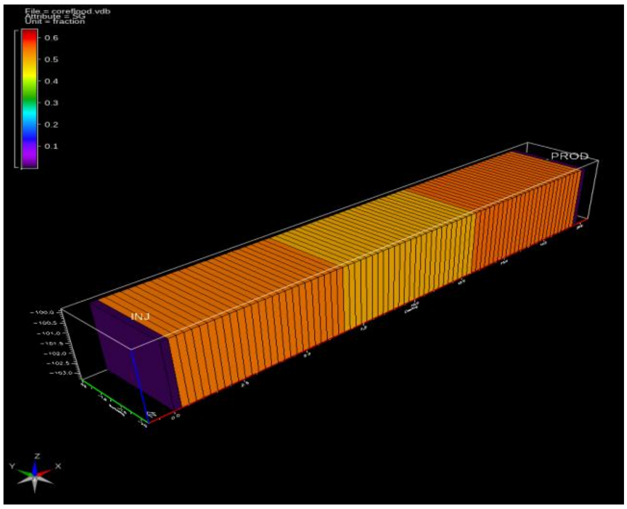

Fig 15: 1D mechanistic model representation

Core dispersivity was estimated from single-phase tracer tests. The measured Peclet number of 50 was represented by 25 grid blocks in each core plug, to match numerical dispersion in the model to the measured physical dispersion, assuming single-point upstream weighting. Rock properties were based on lab measurements. Two wells were defined in the model: an injector on the left side and a producer on the right side. The former injects water at a constant rate of 2 ml/hr, identical to the coreflood. The producer was controlled on bottom hole pressure (BHP). The BHP was reduced at 174 psi per day, the same rate as the coreflood.

Initial water and gas saturations were matched to the experimental data in Fig 9 (green curve), hence the average initial gas saturation is 53%. This is equal to the trapped gas saturation (S_{gr}). As discussed earlier, under depressurisation, remobilisation does not happen until a critical threshold gas saturation (S_{gt}) is reached, at which point gas ganglia reconnect and production begins. Fig. *7* suggests that during the first ~70 hours of depressurisation, no gas was produced from the core plug. During this period, $S_g < S_{gt}$ and gas expands in situ. The value of S_{gt} was estimated from PVT data and was then fine-tuned by simulation to $S_{gt} = 61.1\%$. Fig 16 shows the relative permeability curves used in the model. The rightmost plot was ultimately used to match the experiment: gas relative permeability is zero from S_{gr} to S_{gt} and this causes the gas phase to expand in the core, with no production.

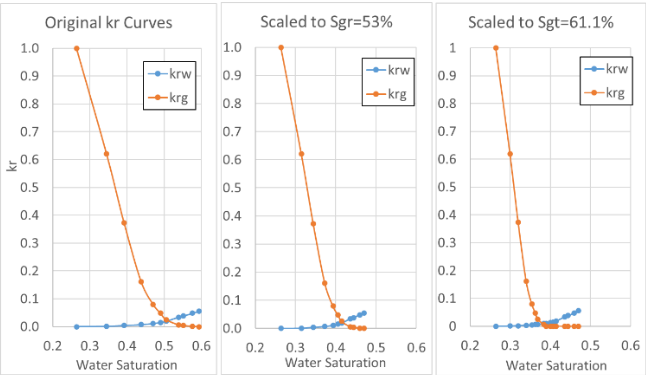

Fig 16: Relative permeability curves. left: original kr from Digital Rocks study (described later); middle: kr scaled to Sgr=53%; right: kr scaled to Sgt=61.1% (used in model matched to Coreflood 1).

The simulation was run for the same time period as the experiment, and the predicted pore pressure and gas production data are compared to the physical coreflood results in Fig. 17 and Fig. 18, respectively. The results show that the model matches pore pressure in the experiment. Cumulative gas production is also in reasonable agreement, with the lab data giving a final gas saturation of 0.61 PV compared to 0.59 PV in the simulation.

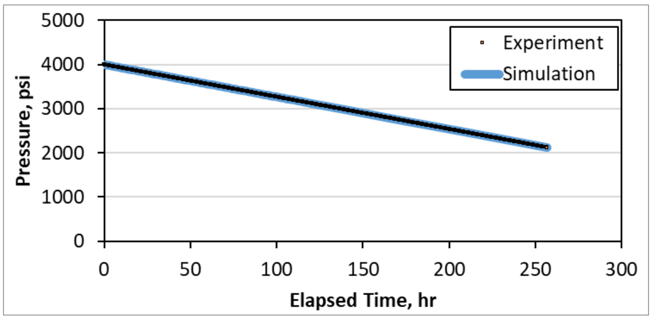

Fig. 17: Experimental and simulated pressure profiles, Coreflood 1.

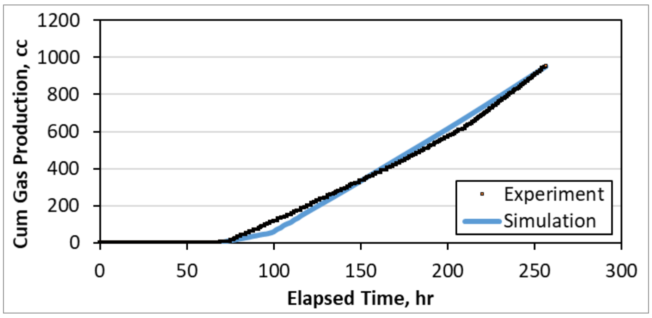

Fig. 18: Cumulative gas production comparison of simulated predictions versus experimental measurements shows agreement to within ~1%

4 Digital Rocks

Minicores were cut from end trims of each of the three coreplugs used in the composite. The samples were micro-CT imaged (at 1.35-1.55 um resolution) for digital rocks physics simulation and analysis. Reservoir properties for these three minicore images showed similar basic properties to the coreflood results, with a porosity of 0.12 and absolute permeability of 45 mD. An extensive sub-voluming characterization workflow, completed on each of the three minicore images and capturing rock property heterogeneity at a representative elementary volume (REV) scale length of approximately six median-sized grains per linear dimension, reveals that spatial variations in rock fabric results in P25-P75 porosity and absolute permeability distributions of (0.095-0.131) v/v and (20-70) mD, respectively. The sub-volume image that best represented the median of the porosity and permeability distributions was chosen to develop the pore scale remobilisation simulation models for the digital experiments, described below.

4.1 Digital Rocks model setup

Following the microCT scan on the chosen mini plug, a 3D model grid was carefully generated using bp's Digital Rocks pore scale image analysis and numerical processing toolkit, to identify an appropriately resolved pore system for N_2-brine remobilisation (pressure depletion) simulations. Fig. 19 presents the 3D tomogram volume and Swi volume generated in preparation for subsequent multiphase simulations.

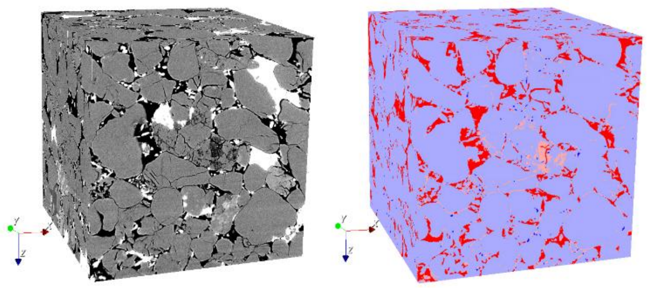

Fig. 19: Tomogram image (left) and rendering of the fluid distribution at the target Swi (right) for the digital grid model for the chosen mini plug. Swi color association: solid (grain) – light blue; microporous volume – dull red; fluid phase – gas: red; fluid phase – brine: blue

The next two sections provide details on the remobilisation simulation methodology and results of the various numerical experiments that mimic the physical test described in Section 2.2.1.

4.2 N_2-brine gas remobilisation simulation method

The DR depressurisation study was executed to replicate the complex reservoir behavior and evaluate the pore scale mechanisms that occur as brine is produced under pressure depletion. The 3D model used in the simulations had dimensions 1.35 mm x 1.35 mm x 1.35 mm. Model porosity was 11.25%. Microporosity increased the total porosity to 12.75%. The digital grid model for porosity is shown below in Fig. 20.

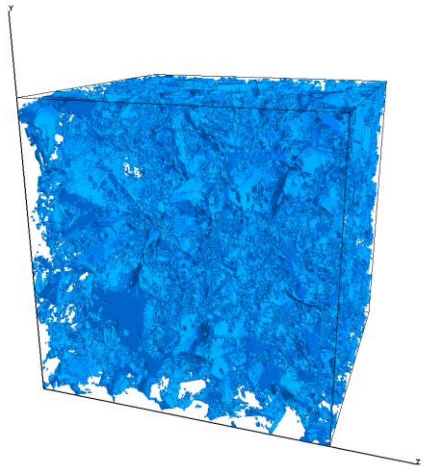

Fig. 20: Digital grid porosity model (blue).

The Direct HydroDynamic (DHD) simulator was used to perform single and multiphase flow modeling on the DR model. The DHD is a multiphase compositional hydrodynamic simulator that is based on the Density Functional Hydrodynamics (DFH) method. This method combines classical thermodynamics and hydrodynamics via constitutive relations with particular expression for the density functional that is based on Helmholtz energy of multiphase multicomponent systems. The system of equations is the same everywhere and phase interfaces are treated by the means of diffuse-interface approach [8].

The DHD simulator was used to perform digital routine core analysis (Digital RCA) [9], digital special core analysis (Digital SCAL) [10, 11, 12] and gas remobilisation modeling using a combination of digital representation of the pore structure, a detailed digital fluid model of reservoir fluids and injectants and rock-fluid interaction. Digital RCA modeled absolute permeability in the 3D model of 56.46 mD.

DHD can handle complex fluids, including complex compositional fluids with phase transitions and variable phase composition, accounting for phase property changes with pressure and temperature, gas solubility in brine and boundary conditions matching experimental coreflooding setups and allowing modeling of the slow rate depressurisation tests.

The 3D model was first used in DHD modelling to establish target gas saturation using unsteady state (USS) waterflooding at multiple rate conditions from gas saturated state at Swi conditions to trapped gas saturation S_{gr}.

Further modeling was then performed using the S_{gr} condition obtained using rate matching to the experimental flow conditions. The model starts at Sgr conditions and represents concurrent brine flow performed at continuously reducing pore pressure and analyses the initially immobile gas phase that increases in volume, reconnects and remobilises as the pore pressure reduces. To test the validity of the DR depressurisation model the resulting data was compared with a laboratory coreflood, described below in 5.1.

5 Digital Rocks Results

5.1 N_2-brine gas remobilisation simulation results

To establish the initial conditions for the gas remobilisation simulation, the unsteady state (USS) waterflood method was used to establish trapped gas saturation in the 3D model at multiple rate conditions from a gas saturated state to trapped gas saturation S_{gr}. The trapped gas saturation at the rate matching lab conditions was 0.52.

The depressurisation test modeling was then performed at 60°C, using live brine and nitrogen properties over the depressurisation range of coreflood 1. The simulation started at 4,000 psi pore pressure, with the nitrogen and brine phases at trapped gas saturation condition. The pore pressure was then gradually reduced to 2300 psi with concurrent brine flow. Gas and water 3D saturations were obtained during the pressure depletion as well as gas saturation changes. Example saturation images at pressures of 4000 psi, 3500 psi, 3000 psi, 2500 psi and 2300 psi are shown below in Fig. 21.

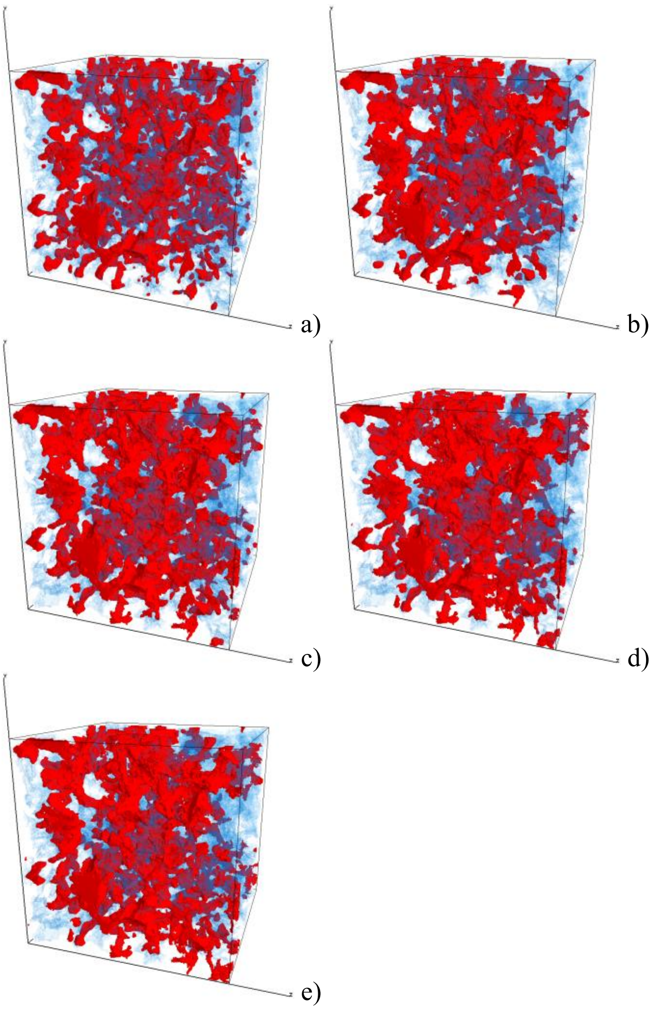

Fig. 21: Gas and brine saturations in the grid model at (a) initial pressure of 4000 psi, (b) 3500 psi, (c) 3000 psi, (d) 2500 psi and (e) 2300 psi. The water phase is shown in blue, gas is shown in red, rock is transparent

Gas production from the pores was analysed and it was established that gas was moving as separate bubbles. Mobilization of gas via discrete bubbles held gas saturations in the core at near constant values, rather than rising to a critical saturation where the gas would become mobile as a continuous phase. The gas saturation increased from Sg = 0.5211 at 4000 psi to Sg = 0.5852 at 3500 psi where gas production started. Gas bubbles started to appear in larger numbers below 3500 psi but no continuous gas phase was observed over the pressure interval studied. After mobilization, gas saturation reduced to the saturation level supported by rock texture and local conditions such that at the final pore pressure of 2,300 psi Sg = 0.5354.

6 Comparison of Digital Rocks Results with Coreflood 1

To verify the DR modeling results, a comparison with Coreflood 1, with its low and constant NCS during depressurization, was made. The coreflood was "digitally twinned" with the coreflood and the results of the physical and digital experiments were compared as follows.

Both experiments consisted of primary imbibition to Sgt from 100 % gas saturation, followed by pressure depletion under constant rate brine flow, with gas production and saturation profiles being recorded. Given the differences in reservoir models (19 cm long stack of core plugs for physical experiment vs. 1.35 mm x 1.35 mm x 1.35 mm cube of voxels for digital simulation) the results were compared based on the gas remobilisation pressure and the subsequent character of gas production.

Based on these two "anchors" there was good consistency between the digital and physical data sets, specifically:

1. Initial trapped gas saturations were very close at 0.52 and 0.53 PV for the coreflood and DR respectively.
2. Both tests started to demonstrate material gas production at practically the same pore pressure: 3501 psi for physical core flow test, and 3500 psi for the digital twin experiment.
3. Mobilised gas was produced by discrete slugs, not continuous flow of gas phase, in both cases.
4. Gas saturations in both DR modeling and the lab experiments rose steadily through the depressurisation by around 6 %.

Both experiments showed gas being remobilised at the same pore pressure, with the same gas production dynamics, despite the differences in the models' size and the degree of variation of properties. This consistency gave the confidence to use the validated DR engine for the main reservoir condition phase of the depletion modelling. More details of the DR process, and application of the model to predict to field behavior at full reservoir conditions with hydrocarbon gas, will be the subject of a future paper.

7 Conclusions & future work

A depressurisation coreflood was run over a 10-day period with continual brine recirculation, representing the process of trapped gas remobilization in a residual gas zone by producing brine. The first coreflood was designed to be a close analogue to the Digital Rocks simulation, in which there was no change in NCS during the depressurisation. During depressurisation from an initial pore pressure of 4,000 psi down to 2,300 psi, 34% of the gas-initially-in-place was produced, and the gas saturation in the core was observed to increase slightly as water relative permeability decreased from 0.025 to 0.016. Gas remained immobile until a substantial reduction in pore pressure (~500 psi) was reached. Gas production was observed as a series of discrete gas bubbles rather than a continuous stream of gas. A reduced order (1D) simulation model of the Coreflood 1 replicated the experimental results very well, indicating a critical gas saturation of 61.1%.

A Digital Rocks twin of the coreflood matched the results remarkably well, predicting the pressure at which gas was remobilized almost exactly. It also predicted gas production in the form of bubbles and not a continuous stream. Despite differences in model scale and geometry, the excellent agreement between physical and digital results provided confidence that the DR approach captured the dominant physics governing residual gas remobilisation.

The validated Digital Rocks workflow was shown to be a robust and practical tool for studying depressurisation behavior under reservoir conditions that are inaccessible to laboratory coreflood equipment. By integrating laboratory experiments, pore-scale simulations, and mechanistic reservoir-scale modelling, this study demonstrates a credible workflow for evaluating the producibility of residual gas zones and for supporting field development decisions where uncertainty around trapped gas behavior is high.

A second coreflood was designed to replicate the reservoir processes more accurately, with increasing NCS as the pore pressure decreased. In this test, gas remobilisation occurred much earlier, after only 100 psi reduction in pore pressure, and recovery was significantly enhanced. More than 77% of the initially trapped gas was produced, despite only a modest (~7%) reduction in absolute permeability due to compaction. These results suggest a critical role for stress-induced pore-scale redistribution and localized pressurization of the fluids (i.e., compaction drive), where mechanical compaction preferentially displaces brine from small pores into larger pores occupied by the non-wetting gas phase and thus promotes enhanced gas connectivity and mobilisation.

To validate a DR depressurisation model for field-scale predictions, where the non-wetting phase is hydrocarbon gas instead of the nitrogen gas tested herein, additional fluid characteristics (e.g., differing phase solubilities and interfacial tension between the brine and gas fluids) will have to be included in the laboratory protocol. With the equipment and testing method challenges overcome, the authors believe that performing a set of more field-realistic corefloods would remove several key uncertainties that presently hinder extrapolating the current findings to field conditions.

Overall, the results show that residual gas remobilisation during depletion is feasible, stress-dependent, and dominated by pore scale mechanisms that are not captured by conventional steady-state relative permeability concepts and reservoir simulators. The combined experimental–digital methodology presented here provides a powerful framework for assessing recovery potential in deep, high-pressure reservoirs and for extending laboratory insights to true reservoir conditions. Future integration opportunities of the underlying Digital Rocks and physical testing technologies will likely include calibration studies to match pore scale simulation results with equivalent laboratory hydrocarbon gas depressurisation experiments under varying NCS, injection rate, and rock quality conditions, with *en vivo* timelapse microCT imaging.

Finally, considering the coreflooding in-situ saturation monitoring, it was surprising that the X-ray based ISSM remains quantitative or close to quantitative even as both pore and confining pressures are reduced. This useful, if counter-intuitive finding will be integrated into updated laboratory protocols to benefit future studies.

7 Acknowledgments

The authors would like to thank Scott Vermeer from Ametek for support and advice on Quizix pump setup and James Brodie (BP) for technical feedback and discussions relating to the corefloods and interpreting the pore scale processes.

References

1. G. Hamon, K. Suzanne, J. Billiotte, V. Trocme., SPE Annual Technical Conference and Exhibition, New Orleans, Louisiana, doi: https://doi.org/10.2118/71524-MS (2001)
2. T.P. Fishlock, R.A. Smith, B.M.Soper, R.W. Wood, SPE Res. Engin., 3:387–94, https://doi.org/10.2118/15455-PA. (1988)
3. R. Moghadasi, F. Basirat, J. Bensabat, C. Doughty, S. McDougall, M.J. Blunt, A. Niemi., 16th Greenhouse Gas Control Technologies Conference (GHGT-16), pp. 23-24 (2022)
4. R. Moghadasi, S. Goodarzi, Y. Zhang, B. Bijeljic, M. J. Blunt, A. Niemi, Advances in Water Resources 179, 104499 (2023)
5. A. Cable, D. Mogford, M Wannell, Society of Core Analysts Annual Symposium Proceedings, SCA2004-29, (2004)
6. D. Olsen, Petrophysics 59, no. 01, 54-61 (2018)
7. P.M.T.M. Schutjens, T.H. Hanssen, M.H.H. Hettema, J. Merour, P. De Bree, J.W.A. Coremans, G. Helliesen, Annual Technical Conference and Exhibition, New Orleans, Louisiana, SPE, pp. 1-12 (2001)
8. IEA, Energy Technology Analysis, Prospects for CO2 Capture and Storage, ISSN: 19901356 https://doi.org/10.1787/19901356 (2004)
9. J. Underschultz, J.E. King, et.al, International Journal of Greenhouse Gas Control, **5 Issue 4**, 922-932 (2011)
10. A. Demianov, O. Dinariev, N. Evseev, Canadian Journal of Chemical Engineering 89, 206–226 (2011)
11. D. Klemin, P. Schlicht, R.E. Distaso, et al., SPE Reservoir Characterization and Simulation Conference and Exhibition, Abu Dhabi, UAE, 24–26 January, SPE-212617-MS. https://doi.org/10.2118/212617-MS (2023)
12. M.R. Dernaika, B. Mansour, M. Konda, D. Klemin, R. Bhakta, M.A. Gibrata, Q. Huang, L. Rouis, G. Ameish, M. Eldali, SPE Caspian Technical Conference and Exhibition, SPE-223478-MS (2024)
13. R. T. Armstrong, A. Georgiadis, H. Ott, D. Klemin, S. Berg, Geophysical Research Letters, Volume 41, Issue 1, January, pp. 55–60 (2014)
14. D. Klemin, S. Masalmeh, A. AlSumaiti, R. Bhakta, M. Dernaika, 38th International Symposium of the Society of Core Analysts, Hannover, Germany, 25-29 August, SCA2025-1013 (2025).